Available online at www.sciencedirect.com
ScienceDirect
Trans. Nonferrous Met. Soc. China 34(2024) 1606−1617
Transactions of Nonferrous Metals Society of China
www.tnmsc.cn

Microstructure and corrosion resistance of Zn−Al/T8 superhydrophobic composite coating on sintered NdFeB magnet

Xiao-hu ZHANG, Jun-ming LUO, Ji-lin XU, Jin CHEN, Jun HUANG, Yong-cun MA, Ming-shan XUE

School of Materials Science and Engineering, Nanchang Hangkong University, Nanchang 330063, China

Received 3 November 2022; accepted 4 May 2023

Abstract: In order to improve the corrosion resistance, the Zn−Al/T8 (2-perfluorooctane ethyl acrylate) superhydrophobic composite coating was prepared on the sintered NdFeB magnet by spin coating method coupled with plasma-enhanced chemical vapor deposition. The results show that the Zn−Al coating is mainly composed of lamellar Zn and Al phases with the thickness of approximately 28 μm. The contact angle of the Zn−Al/T8 coating reaches 151.78° with the rolling angle of 5.13°, indicating that the Zn−Al/T8 coating can provide a superhydrophobic surface. The Zn−Al and Zn−Al/T8 coatings have no significant effect on the magnetic properties of the NdFeB magnets. The Zn−Al coating improves the corrosion resistance of the NdFeB by sacrificing the anode, while the Zn−Al/T8 coating further enhances the corrosion resistance through the superhydrophobic surface. The Zn−Al/T8 composite coating has better salt spray resistance than Zn−Al coating. The Zn−Al/T8 superhydrophobic composite coating is a promising candidate for protecting the sintered NdFeB magnets.

Key words: microstructure; corrosion resistance; sintered NdFeB magnet; Zn−Al coating; superhydrophobic surface; spin coating method; plasma-enhanced chemical vapor deposition

1 Introduction

As the third generation permanent magnet materials, the sintered NdFeB magnets have been widely used in magnetic rail, permanent magnet motor, wind power generation, new energy vehicles, biotechnology, frequency conversion electrical appliances and other fields due to their excellent magnetic properties, such as high remanence, high coercivity, and large maximum magnetic energy product [1−3]. However, the corrosion resistance of the sintered NdFeB magnets is extremely poor, which is attributed to the inherent sintered porous structure and the galvanic effect formed during multiple phases inside the magnets [4−6]. The poor corrosion resistance greatly inhibits the further commercial application of the sintered NdFeB magnets, and the surface protection has become an indispensable process for the sintered NdFeB magnets.

To improve the corrosion resistance of the sintered NdFeB magnets, the main strategies are alloying and coating [7]. Although the alloying method can improve the corrosion resistance of the sintered NdFeB magnets to some extent, it also reduces the magnetic properties of the magnets [8]. Therefore, the coating technology is a more effective method to improve the corrosion resistance of the sintered NdFeB magnets. It mainly includes electroplating [9], electroless plating [10,11], physical vapor deposition [12−14], micro-arc oxidation [15], plasma immersion ion implantation and deposition [16], and cathodic electrophoretic

Corresponding author: Jun-ming LUO, Tel: +86-791-83953271, E-mail: jmluo@nchu.edu.cn;
Ji-lin XU, Tel: +86-791-83863034, E-mail: jlxu@nchu.edu.cn
DOI: 10.1016/S1003-6326(24)66494-0

deposition [17], etc. Among these coatings, the Zn−Al coating as a thermosetting sintered coating has the advantages of high-temperature resistance, good adhesion, and uniform appearance, which has been widely used in the anti-corrosion of the metallic materials [18]. Traditionally, the Zn−Al coatings are mainly prepared by electroplating, and the stability and electrochemical protection of Zn−Al coatings are better than those of zinc and aluminum single-layer coatings [19]. Electroplating equipment is low cost, but it will cause great pollution to the environment if not handled properly. Dacromet coating is a possible alternative coating process. However, it contains Cr^{6+} ions, which has a serious carcinogenic risk. Therefore, scientists at home and abroad widely use chrome-free dacromet coatings, that is, Zn−Al coatings in this work, to avoid the harm of Cr^{6+} [20]. But the existence of the micropores in the Zn−Al coatings seriously affects the enhancement of corrosion resistance [18].

In recent years, superhydrophobic surfaces have been widely used in the fields of photo-catalysis, waterproof, self-cleaning and corrosion resistance due to their excellent hydrophobic properties [21−23]. Generally, the contact angle of the hydrophobic coating is greater than 90°, and the contact angle of the superhydrophobic coating is greater than 150°, coupled with the rolling angle being less than 10° [24]. It is generally believed that the preparation of superhydrophobic surface should meet two conditions at the same time: one is that the surface has a low surface energy, and the other is that the surface has a certain microstructure. In this work, in order to construct the super-hydrophobic surface on the sintered NdFeB magnets to improve the corrosion resistance, the lamellar structure of Zn−Al alloy coating was used as its specific microstructure and the 2-perfluorooctane ethyl acrylate (T8) was used as the low surface energy modifier [25]. On the one hand, the T8 film can effectively cover the micro-defects on the surface of the Zn−Al coating. On the other hand, the T8 film provides a second film layer [26], and lowers the surface energy and forms the superhydrophobic surface. Therefore, the T8 film layer can not only effectively block the penetration of corrosive media such as water and oxygen [27], but also enable water droplets to take away surface pollutants when rolling on the surface of the coating to keep the surface of the coating in a clean state [28,29]. Moreover, the XRD, SEM, VSM, optical contact angle tester, electrochemical corrosion, and salt spray test were employed to investigate the phase and chemical compositions, microstructure, magnetic properties, contact angles, and corrosion resistance of the superhydrophobic composite coating, respectively.

2 Experimental

2.1 Sample preparation

Unmagnetized N35 sintered NdFeB magnets (provided by Jiangxi JLMAG Rare-Earth Co., Ltd., China) were used as the substrate. The sintered NdFeB magnets were cut into 13 mm × 13 mm × 3 mm and sandblasted with 0.6−0.85 mm white corundum, in which the sandblasting angle was 65°−80°, the sandblasting pressure was 0.45 MPa, and the sandblasting distance was 90 mm. The Zn−Al coating was prepared by spin coating method. The sandblasted NdFeB was put into the Zn−Al metal slurry (manufactured by Ammet (China) Chemical Co., LTD) for approximately 15 s, and then rotated clockwise at speed of 450 rad/s for 15 s, followed by rotating counterclockwise at speed of 450 rad/s for other 15 s. Subsequently, the samples were pre-baked in a vacuum chamber at 110 °C for 10−20 min, and then sintered in a vacuum tube furnace at 280 °C for 40 min. Finally, the thermosetting Zn−Al coating was obtained. The Zn−Al coated NdFeB samples were then placed into the coating chamber, and the T8 film was prepared by plasma-enhanced chemical vapor deposition (PECVD, SQ−101, Guangdong Suqun New Material Co. LTD, China).

2.2 Microstructural characterization

The surface and cross-sectional morphologies of the samples were observed by scanning electron microscope (SEM, FEI Nova Nano SEM450, USA). The phase composition of the samples was analyzed by X-ray diffraction (XRD, Bruker D8 Advance, Germany) using a Cu K_α radiation. The contact angle and rolling angle of the samples were studied by optical contact angle tester (DSA100, KrüSS, Germany), and the average value was obtained after five measurements. The magnetic properties of the coated and uncoated NdFeB magnets were analyzed by a physical property measurement system (PPMS, Quantum Design) equipped with a 9 T vibrating

sample magnetometer (VSM).

2.3 Corrosion resistance tests

A CHI 660E electrochemical workstation (Shanghai Chenhua Instrument Co., Ltd., China) was employed to evaluate the open circuit potential (OCP), potentiodynamic polarization, and electrochemical impedance spectroscopy (EIS) of samples in 3.5 wt.% NaCl solution at room temperature. The traditional three-electrode electrochemical cell was used, in which a saturated calomel electrode (SCE) was used as the reference electrode, a platinum plate was used as the counter electrode, and the samples with an exposed area of 1 cm^2 was used as the working electrode. Before potentiodynamic polarization and electrochemical impedance tests, the working electrodes were immersed in 3.5 wt.% NaCl solution for 30 min to stabilize the electrodes, and the OCP was recorded continuously. The EIS was measured in the frequency range from 10^{-2} to 10^5 Hz with an amplitude of 10 mV. The potentiodynamic polarization curves were measured at the scanning rate of 1 mV /s, and the corrosion potential (φ_{corr}) and corrosion current density (J_{corr}) of coated and uncoated samples were obtained by the Tafel extrapolation method.

The corrosion behavior of the coated NdFeB samples was also investigated by salt spray test. Prior to testing, the coated samples were encapsulated with AB glue to expose an area of approximately 1 cm^2. The salt spray test was carried out in a salt spray chamber according to ASTMB−117. SEM was employed to observe the morphologies of corrosion products.

3 Results and discussion

3.1 Microstructure of composite coatings

Figure 1 shows the XRD patterns of uncoated, Zn−Al coated and Zn−Al/T8 coated NdFeB samples. Both of the Zn−Al coating and the Zn−Al/T8 coating are mainly composed of Zn and Al phases, which are the same as the Dacromet coatings system [30]. The diffraction peaks located at 2θ=36.27°, 38.99°, 43.23°, 54.34°, 70.06°, and 70.66° correspond to the (002), (100), (101), (102), (103), and (110) crystal planes of Zn phase, respectively. The diffraction peaks located at 2θ=44.87° and 65.23° correspond to the Al phase. No diffraction peaks of NdFeB substrate can be detected in the Zn−Al coated and the Zn−Al/T8 coated samples, indicating that the coatings are dense and thick enough to shield the signal from the NdFeB substrate. The diffraction intensity of Zn phase is much higher than that of Al phase, indicating that Zn is the dominant phase in the Zn−Al coating, greatly consistent with the original Zn−Al metal slurry. However, due to the presence of T8 film, the diffraction peak intensities of Zn and Al phases in the Zn−Al/T8 coated sample are slightly lower than that of the Zn−Al coated sample. This also further proves the successful application of the T8 film on the surface of the Zn−Al coating.

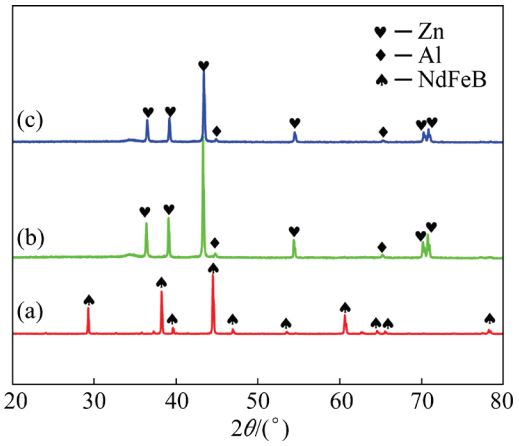

Fig. 1 XRD patterns of uncoated (a), Zn−Al coated (b), and Zn−Al/T8 coated (c) samples

The surface and cross-sectional morphologies of the Zn−Al coated and Zn−Al/T8 coated samples are shown in Fig. 2. The Zn−Al coating exhibits silver-white appearance, and the T8 film does not change its macroscopic color significantly. Combined with the surface and cross-sectional morphologies, it can be seen that the Zn−Al coating is mainly composed of micrometer lamellar structures superimposed on each other. There are some defects between the lamellar structures, such as gaps, cracks and pores. Defects in coatings are mainly due to the volatilization of solvents, especially water [31]. The corrosive medium can penetrate to the NdFeB substrate through these gaps and cracks, which will inevitably lead to a decrease in the corrosion resistance of the Zn−Al coating [32]. However, these defects form a labyrinth-like structure inside the coating, which delays the time for the corrosive medium to reach the substrate. Moreover, it can also be seen from the

cross-sectional morphology that the thickness of Zn−Al coating is approximately 28 μm, and the interface between the coating and the substrate is well bonded.

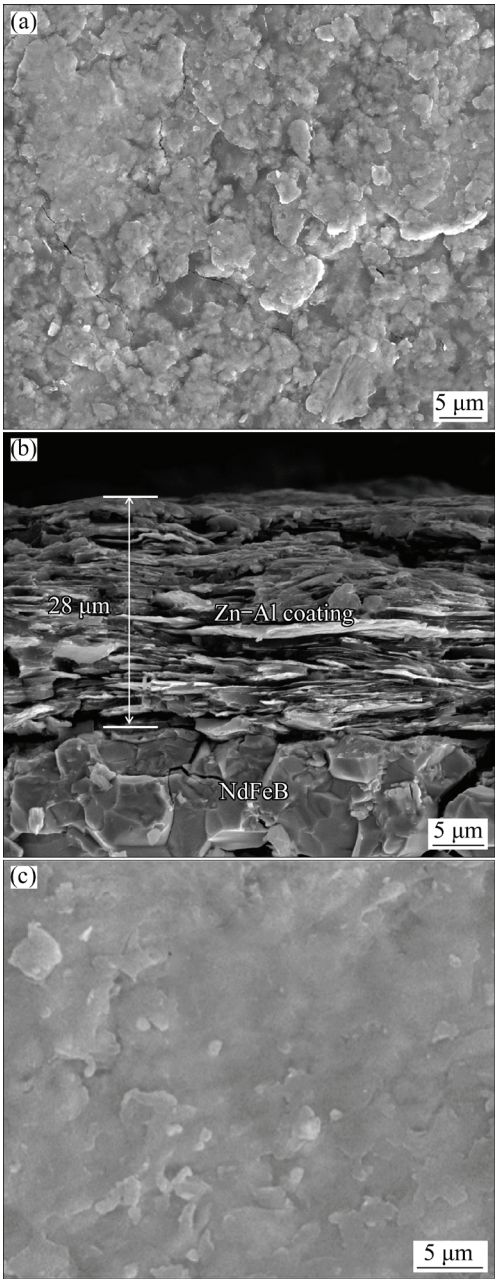

Fig. 2 Surface and cross-sectional morphologies of Zn−Al coated (a, b) and Zn−Al/T8 coated (c) samples

In order to seal the defects on the surface of the Zn−Al coating and form a superhydrophobic surface, a T8 film was prepared on the surface of the Zn−Al coating. The surface of Zn−Al/T8 composite coating still shows lamellar structure, while there are no obvious cracks and pores on the surface, indicating that the sealing effect of the T8 film is good. Because the T8 film is very thin, the cross-sectional morphology (not shown in this paper) of Zn−Al/T8 composite coating is not significantly different from that of the Zn−Al coating. The elemental composition of the Zn−Al coated and Zn−Al/T8 coated samples is listed in Table 1. By comparing the composition of the two coated samples, it can be seen that the contents of the C and F elements on the Zn−Al/T8 coated sample increase significantly, while the contents of Zn and Al elements decrease significantly, further indicating the successful deposition of the T8 film.

Table 1 Elemental contents of Zn−Al coated and Zn−Al/T8 coated samples (wt.%)

Sample	C	O	F	Al	Si	Ti	Zn
Zn−Al	8.34	13.81	−	7.77	4.17	1.85	64.06
Zn−Al/T8	25.00	8.99	15.70	4.03	5.50	1.05	39.66

3.2 Contact angle of coated and uncoated samples

The contact angles of the uncoated, the Zn-Al coated, and the Zn−Al/T8 coated samples are shown in Fig. 3. The contact angle of the uncoated NdFeB substrate is only (41.81±1.25)°, while the Zn−Al coated sample can reach (117.83±2.19)°. The Zn−Al coating changes NdFeB magnets from hydrophilic surface to hydrophobic surface. The contact angle of Zn−Al/T8 coated sample is up to (151.778±1.29)°, and the rolling angle is only (5.13±1.25)°, which fully meets the requirements of superhydrophobic surfaces [24]. The rough surface and inherently porous structure give the NdFeB substrate high surface energy, which provides high energy for liquid stretching, resulting in low contact

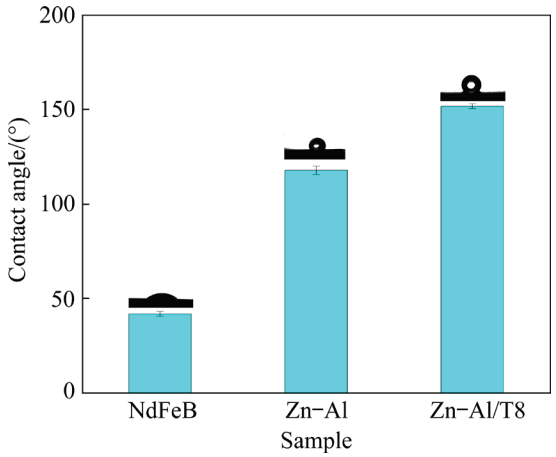

Fig. 3 Contact angles of uncoated, Zn−Al coated, and Zn−Al/ T8 coated NdFeB samples

angles and high hydrophilicity. The excellent hydrophobicity of the Zn−Al coating may be attributed to the ZnO film formed on the Zn surface [33]. Fluorides are often used as hydrophobic modified reagents to construct the superhydrophobic surfaces due to their lower surface energy, such as FP, PDP and TFOS [34−36]. Therefore, the lamellar surface morphology of the Zn−Al coating coupled with the modification of low surface energy of the T8 film results in the formation of the superhydrophobic surface.

3.3 Magnetic properties of coated and uncoated NdFeB samples

To study the effect of the Zn−Al coating and Zn−Al/T8 coating on the magnetic properties of the sintered NFeB magnets, the hysteresis loops of the uncoated and coated samples were tested, and the results are shown in Fig. 4 and Table 2. The hysteresis loops of the uncoated NdFeB and the coated samples are similar and almost coincide, indicating that the coatings have no significant effect on the magnetic properties of the NdFeB magnets. It can be seen from Table 2 that the coercivity (H_{ci}) of the coated samples is slightly lower than that of the NdFeB magnets, in which the Zn−Al coated sample only decreases by 0.42%, and the Zn−Al/T8 coated sample decreases by 2.11%. While the remanence (B_r) of the coated samples increases slightly, in which the Zn−Al coated sample increases by 0.76%, and the Zn−Al/T8 coated sample increases by 1.52%. Compared with the uncoated sample, the maximum energy product ($(BH)_{max}$) of the Zn−Al coated sample increases by 1.27%, and that of the Zn−Al/T8 coated sample

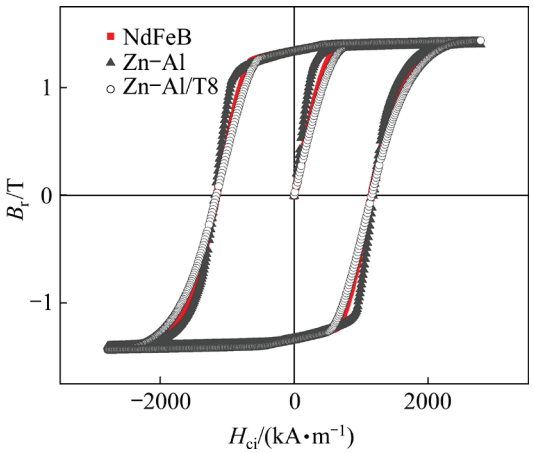

Fig. 4 Hysteresis loops of uncoated, Zn−Al coated, and Zn−Al/T8 coated samples

Table 2 Magnetic properties of uncoated, Zn−Al coated, and Zn−Al/T8 coated samples

Sample	H_{ci}/(kA·m^{-1})	B_r/T	$(BH)_{max}$/(kJ·m^{-3})
Uncoated NdFeB	1186	1.32	316
Zn−Al coated NdFeB	1181 (−0.42%)	1.33 (0.76%)	312 (1.27%)
Zn−Al/T8 coated NdFeB	1161 (−2.11%)	1.34 (1.52%)	322 (1.89%)

increases by 1.89%. However, many other coatings prepared on the sintered NdFeB magnets would lead to a decrease in magnetic properties. The high-entropy alloy coating prepared by HVOF on the NdFeB magnets reduces the maximum energy product by 2.34% [37]. AlN/SiC bilayer films were prepared on the NdFeB magnet by magnetron sputtering, which resulted in the decrease of coercivity by 11.22% [38]. Therefore, the coatings in this work have no significant effect on the magnetic properties of the sintered NdFeB magnets and will not affect the subsequent use.

3.4 Corrosion behavior of coated and uncoated NdFeB samples

Figure 5 shows optical photographs and SEM images of the Zn−Al coated and Zn−Al/T8 coated samples before and after the salt spray test for 504 h. Before salt spray test, both of the Zn−Al coated and Zn−Al/T8 coated samples (Figs. 5(a, b)) exhibit silver-white with metallic luster, without significant difference, indicating that the T8 film has no significant effect on the appearance of Zn−Al coating. After 504 h salt spray test, partial damage on the surface of the Zn−Al coated sample (Fig. 5(c)) can be observed, but no brown rust spots corroded by the NdFeB substrate can be found. This indicates that the Zn−Al coating has excellent sacrificial anode protection effect. The surface of the Zn−Al/T8 coated sample (Fig. 5(d)) can remain relatively intact with some wrinkles, indicating that the T8 film or superhydrophobic surface can further improve the corrosion resistance of the NdFeB magnets. SEM analysis was carried out after the salt spray test for 504 h. It can be found from Fig. 5(e) that the Zn−Al coating is obviously dissolved and peeled off, and the integrity of the coating is seriously damaged. While the surface of Zn−Al/T8 coated sample (Fig. 5(f)) is relatively intact, and no large damage of the Zn−Al coating occurs. However,

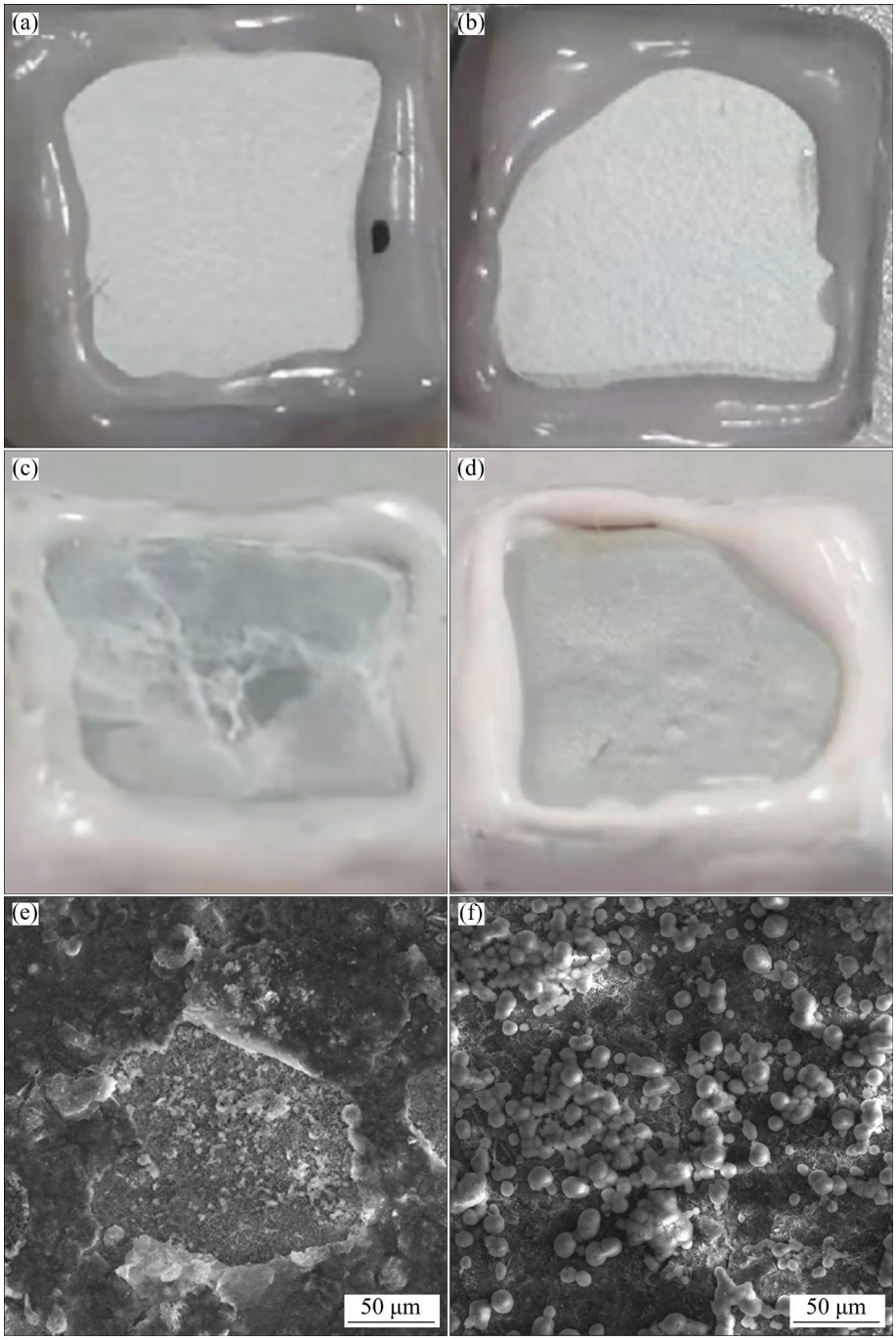

Fig. 5 Optical photographs (a−d) and SEM images (e, f) of Zn−Al coated (a, c, e) and Zn−Al/T8 coated (b, d, f) samples before (a, b) and after (c−f) salt spray test for 504 h

the integrity of the T8 film was also damaged and some spherical particles can be observed on the surface. According to the analysis of EDS, the spherical particles should be ZnO. In general, the Zn−Al/T8 composite coating can effectively improve the salt spray resistance of the sintered NdFeB magnets.

The open circuit potential (OCP)−time curves of the uncoated and coated samples in 3.5 wt.% NaCl solution are shown in Fig. 6. Longer immersion time can provide enough time for the solution to diffuse [39]. To obtain a more stable OCP curve, the coated and uncoated samples were subjected to an OCP test in 3.5 wt.% NaCl solution for 1800 s. It can be seen from Fig. 6 that the OCP values of all samples are stabilized after 1800 s. Generally speaking, the level of potential reflects the corrosion thermodynamics tendency. The Zn−Al

coated sample has a lower potential than the NdFeB substrate and is more prone to corrosion, which can play the role of a sacrificial anode to protect the cathode [40]. The potential of the Zn−Al/T8 coated sample is much higher than that of the NdFeB substrate, indicating that the Zn−Al/T8 coating significantly reduces the corrosion thermodynamics tendency of the sintered NdFeB magnets, which is attributed to the excellent superhydrophobicity of the composite coating. As a protective coating, the Zn−Al/T8 superhydrophobic composite coating can prevent water and oxygen from entering into the Zn−Al coating and the NdFeB substrate.

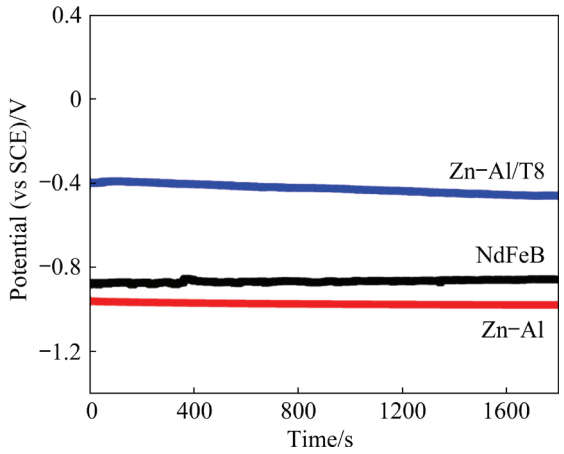

Fig. 6 OCP−time curves of uncoated and coated NdFeB samples in 3.5 wt.% NaCl solution

The potentiodynamic polarization curves of the uncoated, Zn−Al coated, and Zn−Al/T8 coated NdFeB samples in 3.5 wt.% NaCl solution are shown in Fig. 7, and the corrosion results are listed in Table 3. The phenomenon of metal dissolution can be clearly seen in the anodic region of the potentiodynamic polarization curves of the uncoated and Zn−Al coated samples, while the anodic region of the Zn−Al/T8 coated sample exhibits a certain passivation area (−0.3 to 0.6 V). Compared with the uncoated and Zn−Al coated samples, the whole polarization curve of the Zn−Al/T8 coated sample moves towards high potential and low current density, indicating that the Zn−Al/T8 coated sample has better corrosion resistance. On the other hand, the Zn−Al coated sample has more negative corrosion potential and lower corrosion current density compared to the uncoated NdFeB sample. Although Zn−Al coated samples have higher thermodynamic corrosion tendency (more negative φ_{corr}), they also have lower kinetic corrosion rate (lower J_{corr}), indicating that the Zn−Al coated sample has better corrosion resistance than the uncoated NdFeB sample. It can be seen from Table 3 that the corrosion potential of Zn−Al/T8 coated sample is 203 mV higher than that of the uncoated sample, and the corrosion current density is 4.171×10^{-6} A/cm^2, nearly an order of magnitude lower than that of the uncoated NdFeB sample. The corrosion potential of the Zn−Al coated sample is 145 mV lower than that of the uncoated sample, so the Zn−Al coating is preferentially corroded, which provides the driving force for the sacrificial anode to protect cathode [41]. The corrosion current density of the Zn−Al coated is much lower than that of the uncoated sample, which can be judged that the Zn−Al coated sample can increase the corrosion resistance of NdFeB magnets.

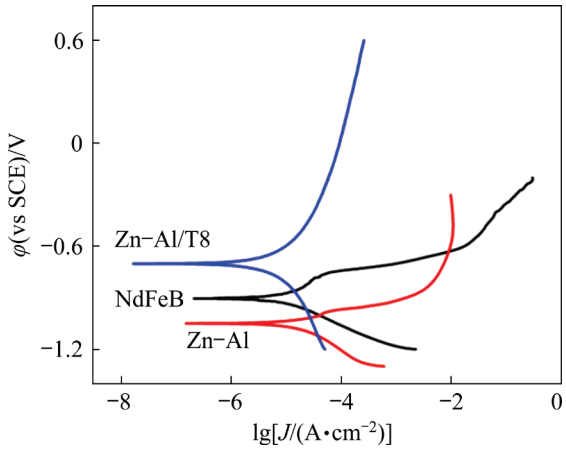

Fig. 7 Potentiodynamic polarization curves of uncoated, Zn−Al coated, and Zn−Al/T8 coated NdFeB samples in 3.5 wt.% NaCl solution

Table 3 Corrosion results of uncoated, Zn−Al coated, and Zn−Al/T8 coated NdFeB samples in 3.5 wt.% NaCl solution

Sample	φ_{corr}(vs SCE)/V	J_{corr}/(A·cm^{-2})
NdFeB	−0.905	1.730×10^{-5}
Zn−Al	−1.050	9.575×10^{-6}
Zn−Al/T8	−0.702	4.171×10^{-6}

Corrosion protection efficiency (η) is always used to evaluate the corrosion resistance of the coated samples, and its calculation formula is as follows [42]:

$$\eta=\frac{J_{corr}^{0}-J_{corr}}{J_{corr}^{0}}\times100\%$$

where J^0_{corr} and J_{corr} represent the corrosion current densities of the uncoated and coated samples, respectively. After calculation, the corrosion protection efficiencies of the Zn−Al coating and the Zn−Al/T8 coating are 44.65% and 75.89%, respectively. The Zn−Al/T8 coating has higher corrosion protection efficiency and better anti-corrosion effect, which further proves its excellent corrosion resistance. The mechanism of the anti-corrosion effect of the Zn−Al coating is mainly due to the barrier effect of Al and Zn and the protection of the substrate by the sacrificial anode. But the existence of the micro-defects on the surface of the Zn−Al coating makes it difficult to further increase the corrosion resistance of the coated sample. The T8 film in the Zn−Al/T8 coating can cover and seal the micro-effects of the Zn−Al coating. On the other hand, the corrosive media such as water and oxygen are blocked outside the Zn−Al/T8 due to its excellent superhydrophobicity. Both of these can greatly improve the corrosion protection efficiency of the Zn−Al/T8 coating.

Figure 8 shows the EIS diagrams and the fitting results of the coated and uncoated NdFeB samples. In Nyquist plots (the insert of Fig. 8(a)), both the NdFeB substrate and the Zn−Al coated sample exhibit a semicircular shape in the high frequency region. While the Nyquist plot of the Zn−Al/T8 coated sample consists of a semicircular-shaped capacitive loop in the high frequency region and a diffusion impedance in the low frequency region. The capacitive loop radius of the Zn−Al/T8 coated sample is significantly larger than those of the NdFeB substrate and the Zn−Al coated sample, indicating an increase in corrosion protection. The Bode plots (Fig. 8(b)) also in intuitively reveal that the sequence of the absolute impedance value ($|Z|_{f=0.01\ Hz}$) is $2.368\times10^4\ \Omega\cdot cm^2$ (Zn−Al/T8 coated sample) > $1.171\times10^3\ \Omega\cdot cm^2$ (NdFeB) > $5.000\times10^2\ \Omega\cdot cm^2$ (Zn−Al coated sample), demonstrating that the Zn−Al/T8 composite coating exhibits the best corrosion resistance.

To further investigate the corrosion protection behavior, three equivalent circuit models are used to evaluate the EIS data for the tested samples, as shown in Fig. 9. During the fitting process, all of the Chi-square values are within 10^{-4}, indicating that fitting results are reasonable and credible. In these equivalent circuits, R_s is the solution resistance,

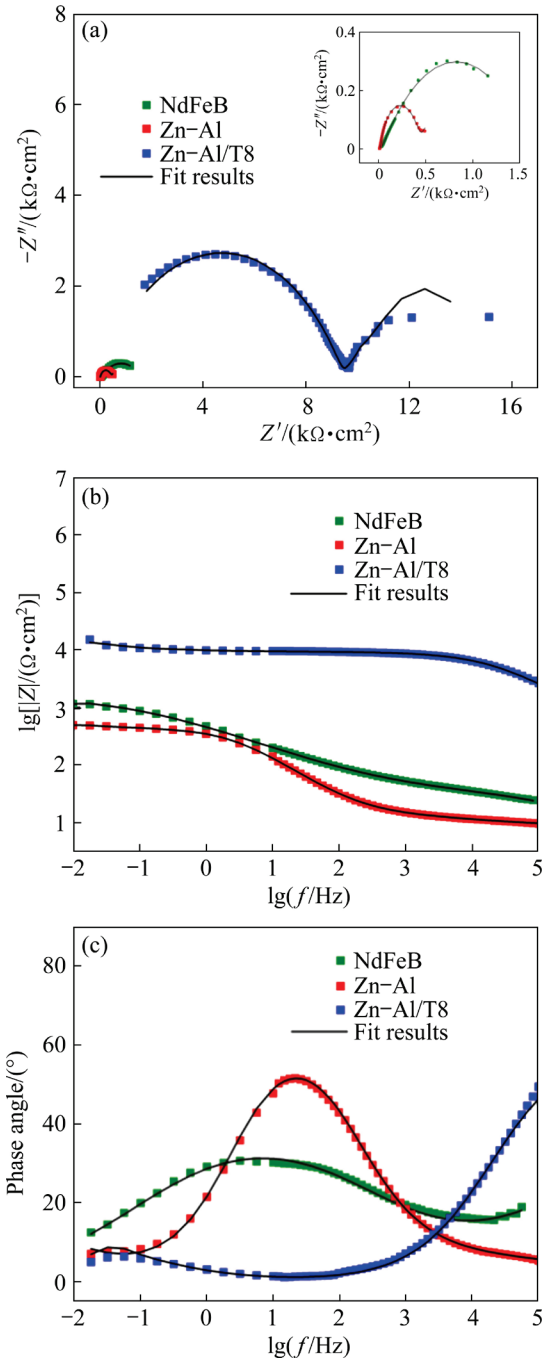

Fig. 8 EIS and fitting results of uncoated, Zn−Al coated, and Zn−Al/T8 coated samples in 3.5 wt.% NaCl solution: (a) Nyquist plots; (b) Bode plots of $|Z|$ vs frequency; (c) Bode plots of phase angle vs frequency

and R_{ct} is the charge transfer resistance. Due to the heterogeneous and rough surface of the samples, the constant phase elements (CPE) are usually introduced into these models to replace the ideal capacitor. Normally, CPE_{dl} is the capacitance of the double layer at the electrolyte/sample interface. Thus, R_{ct} and CPE_{dl} represent the charge transfer

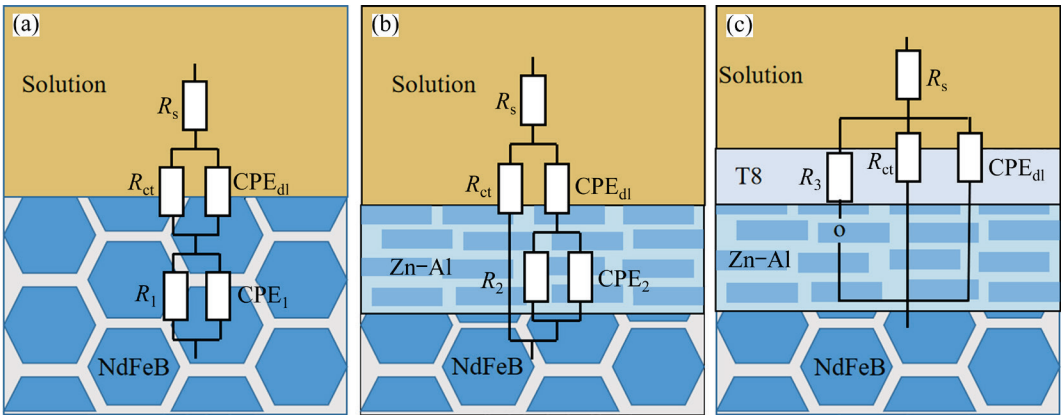

Fig. 9 Equivalent circuits for EIS of tested samples in 3.5 wt.% NaCl solution: (a) Uncoated NdFeB sample; (b) Zn−Al coated sample; (c) Zn−Al /T8 coated sample

Table 4 Fitting results of EIS plots of uncoated, Zn−Al coated, and Zn−Al/T8 coated NdFeB samples in 3.5 wt.% NaCl solution

Sample	CPE_{dl}/ ($\Omega^{-1}\cdot cm^{-2}\cdot s^n$)	n	R_{ct}/ ($\Omega\cdot cm^2$)	CPE_1/ ($\Omega^{-1}\cdot cm^{-2}\cdot s^n$)	n_1	R_1/ ($\Omega\cdot cm^2$)
Uncoated NdFeB	7.738×10^{-4}	0.8	1583	7.212×10^{-5}	0.8	35.74
Zn−Al coated	1.675×10^{-4}	0.78	467	–	–	–
Zn−Al/T8 coated	4.238×10^{-8}	0.669	22750	–	–	–
Sample	CPE_2/ ($\Omega^{-1}\cdot cm^{-2}\cdot s^n$)	n_2	R_2/ ($\Omega\cdot cm^2$)	R_3/ $\Omega\cdot cm^2$	Yo/ ($\Omega^{-1}\cdot cm^{-2}\cdot s^{0.5}$)	B
Uncoated NdFeB	–	–	–	–	–	–
Zn−Al coated	1.845×10^{-5}	0.643	6.758	–	–	–
Zn−Al/T8 coated	–	–	–	16100	1.802×10^{-4}	4.343

process at the electrolyte/sample interface. R_1 and CPE_1 represent the resistance and capacitance of the substrate corrosion products, respectively. R_2 and CPE_2 represent the resistance and capacitance of the corrosion product of the Zn−Al coating, respectively. For the Zn−Al/T8 composite coating, due to the barrier effect of the T8 film, the corrosion products formed at the small defects of the Zn−Al coating are not easily transferred or diffused into the solution. According to diffusion theory, the finite length diffusion element of the cotangent hyperbolic diffusion impedance, O, is suitable in this study [16].

The fitting data of the EIS results are listed in Table 4, in which n is the CPE index ($0\leq n\leq1$) [43,44], and both of the Y_O and B are the O indexes [16]. Among these fitting parameters, R_{ct} is closely related to the corrosion performance of the coatings, which is often employed to evaluate the corrosion resistance of the samples during the corrosion process. The larger the value of R_{ct} is, the more difficult it is for the charge to transfer at the interface. The R_{ct} value of the Zn−Al coating ($4.670\times10^2\ \Omega\cdot cm^2$) is lower than that of the uncoated NdFeB sample ($1.583\times10^3\ \Omega\cdot cm^2$), indicating that the Zn−Al coating can play a good role of sacrificial anode. The R_{ct} value of the Zn−Al/T8 composite coating ($2.275\times10^4\ \Omega\cdot cm^2$) is much larger than that of the uncoated NdFeB sample, meaning that the composite coating has a good protective effect on the NdFeB magnets. The EIS fitting results are in good agreement with the potentiodynamic polarization curves.

4 Conclusions

(1) The Zn−Al/T8 superhydrophobic composite coating is successfully prepared on the sintered NdFeB magnets by spin coating method coupled with plasma-enhanced chemical vapor deposition. The Zn−Al coating is mainly composed of metallic Zn and Al phases with lamellar structure.

The T8 film has no significant effect on the surface morphology and thickness of the Zn−Al coating.

(2) The Zn−Al/T8 composite coating shows excellent superhydrophobility with the contact angle of 151.78° and rolling angle of 5.13°. Both the Zn−Al and Zn−Al/T8 coatings have no significant effect on the magnetic properties of the sintered NdFeB magnets.

(3) The Zn−Al coating protects the sintered NdFeB substrate by sacrificing anode mode, while the Zn−Al/T8 composite coating greatly improves the corrosion resistance of the substrate due to the formation of a superhydrophobic surface. The Zn−Al/T8 superhydrophobic coating has excellent salt spray resistance and electrochemical corrosion resistance.

CRediT authorship contribution statement

Xiao-hu ZHANG: Formal analysis, Investigation, Methodology, Visualization, Writing − Review & editing; **Jun-ming LUO:** Formal analysis, Funding acquisition, Writing − Review & editing; **Ji-lin XU:** Conceptualization, Formal analysis, Funding acquisition, Investigation, Methodology, Writing − Original draft, Writing − Review & editing; **Jin CHEN:** Investigation, Writing − Original draft; **Jun HUANG**: Methodology, Visualization; **Yong-cun MA:** Methodology, Software; **Ming-shan XUE:** Conceptualization, Visualization.

Declaration of competing interest

The authors declare that they have no known competing financial interests or personal relationships that could have appeared to influence the work reported in this paper.

Acknowledgments

The authors gratefully acknowledge the financial support from the National Natural Science Foundation of China (No. 52161040), the Major Science and Technology Research and Development Project of Jiangxi Province (No. 20203ABC28W006), the Natural Science Foundation of Jiangxi Province, China, (No. 20202ACBL214011), and Key Project of “Science and Technology to Promote Mongolian Development”, China (No. XM2021BT03).

References

[1] PRASHANTH N A. Flux maximization in wind turbine permanent magnet synchronous generator made of NdFeB permanent magnets [J]. Materials Today: Proceedings, 2022, 49(3): 731−737.

[2] YANG Zhong-nian, WANG Cui, ZHANG Yan, XIE Yan. Electroplating mechanism of nanocrystalline NdFeB film [J]. Transactions of Nonferrous Metals Society of China, 2015, 25(3): 832−837.

[3] ZHANG Ting-yu, YUAN Zhang-fu, WANG Rong-yue, MA Bo-wen, MEI Lu, ZHAO Hong-xin. Effect of alloy composition on wetting behavior of Sn−Co−La alloy on NdFeB substrate [J]. Physica B: Condensed Matter, 2022, 636: 413886.

[4] SU Xun-wen, ZHU Li-qun, LI Wei-ping, CHEN Hai-ning, CAO Rui, LIU Hui-cong. Effect of alumina sol on formation and properties of electrodeposited zinc coatings on NdFeB magnet [J]. Surfaces and Interfaces, 2020, 21: 100776.

[5] CHEN Jing, YANG Hong-yi, XU Guang-qing, ZHANG Peng-jie, LV Jun, SUN Wei, LI Bing-shan, HUANG Jun, WANG Dong-mei, SHU Xia, WU Yu-cheng. Rare earth passivation and corrosion resistance of zinc coated NdFeB magnets [J]. Journal of Rare Earths, 2022, 40(2): 302−308.

[6] ZHANG Kuan-kuan, FAN En-dian, HE Jian, LI Xiao-gang, HUANG Yun-hua. Long-term effects of electrochemical corrosion on magnetic properties of sintered NdFeB magnets [J]. Journal of Magnetism and Magnetic Materials, 2021, 538: 168309.

[7] HE Wen-ting, ZHU Li-qun, CHEN Hai-ning, NAN Hai-yang, LI Wei-ping, LIU Hui-cong, WANG Yan. Electrophoretic deposition of graphene oxide as a corrosion inhibitor for sintered NdFeB [J]. Applied Surface Science, 2013, 279: 416−423.

[8] WANG Zhuang, LIU Wei-Qiang, ZHANG Dong-tao, YUE Ming, HUANG Xiu-lian, LI Xu-liang. Enhancement of corrosion resistance in sintered Nd−Fe−B permanent magnet doping with different $CuZn_5$ contents [J]. Rare Metals, 2017, 36: 812−815.

[9] JIANG Wei, SHEN Li-da, WANG Kai, XU Ming-yang. TIAN Zong-jun. Study on Ni−Ni(S)−Ni(P) multilayer coating by friction-assisted jet electroplating on sintered NdFeB [J]. Journal of Alloys and Compounds, 2019, 787: 1089−1096.

[10] WANG Yao, DENG Yu-zhou, MA Yuan-tai, GAO Fei. Improving adhesion of electroless Ni−P coating on sintered NdFeB magnet [J]. Surface and Coatings Technology, 2011, 206(6): 1203−1210.

[11] YAN M, YING H G, MA T Y. Preparation of coatings with high adhesion strength and high corrosion resistance on sintered Nd−Fe−B magnets through electroless plating [J]. Materials Chemistry and Physics, 2009, 113(2/3): 764−767.

[12] CHEN E, PENG K, YANG W L, ZHU J J, LI D Y, ZHOU L P. Effects of Al coating on corrosion resistance of sintered NdFeB magnet [J]. Transactions of Nonferrous Metals Society of China, 2014, 24(9): 2864−2869.

[13] HUANG Jun, LIU Qing, YANG Zhen-yu, XU Guang-qing, ZHANG Peng-jie, LV Jun, SUN Wei, LI Bing-shan, WANG Dong-mei, WU Yu-cheng. Densification and anticorrosion performances of vacuum evaporated aluminium coatings on NdFeB magnets [J]. Journal of Rare Earths, 2021, 39(10): 1238−1245.

[14] LIN Yi-cheng, ZHU Qi-hang, ZHENG Bi-zhang, HU Fang-qin, YANG Li-jing, SONG Zhen-lun, XU Cheng, LI Zhi-feng. Effect of titanium addition on structure, corrosion resistance and mechanical properties of aluminum coatings

on NdFeB by ion-beam-assisted magnetron sputtering [J]. Vacuum, 2020, 181:109642.

[15] CHEN J, XU J L, HUANG J, DAI L, XUE M S, LUO J M. Corrosion resistance of T-ZnO_w/PDMS-MAO composite coating on the sintered NdFeB magnet [J]. Journal of Magnetism and Magnetic Materials, 2021, 534: 168049.

[16] WU Hao, XIAO Shu, CHEN Dong-lai, QASIM A M, DING Ke-jian, WU Guo-song, CHU P K. Effects of diamond-like carbon film on the corrosion behavior of NdFeB permanent magnet [J]. Surface and Coatings Technology, 2017, 312: 66−74.

[17] XU J L, ZHONG Z C, HUANG Z X, LUO J M. Corrosion resistance of the titania particles enhanced acrylic resin composite coatings on sintered NdFeB permanent magnets [J]. Journal of Alloys and Compounds, 2013, 570: 28−33.

[18] HU Hui-li, LI Ning, CHENG Jin-ning, CHEN Li-jiao. Corrosion behavior of chromium-free dacromet coating in seawater [J]. Journal of Alloys and Compounds, 2009, 472(1/2): 219−224.

[19] XIAO Yu-xing, JIANG Xin-hua, XIAO Yi-de, MA Liang-li. Research on Zn−Al15 thermal spray metal coating and its organic painting composite system protection performance [J]. Procedia Engineering, 2012, 27: 1644−1653.

[20] CAI Jia-bin, SHI Xiao-jie, SONG Jian, SONG Jun-jun, JING Fu-qi, XIAO Qi-hong. Comprehensive performance test and analysis of graphene-enhanced chromium-free Dacromet coating [J]. Corrosion Reviews, 2020, 38(5): 445−461.

[21] LI Hao, XIN Lei, ZHANG Kai, YIN Xiao-li, YU Si-rong. Fluorine-free fabrication of robust self-cleaning and anti-corrosion superhydrophobic coating with photocatalytic function for enhanced anti-biofouling property [J]. Surface and Coatings Technology, 2022, 438: 128406.

[22] WANG Yu, ZHANG Qian, LI Ping-ping, HUANG Jin-tian. A durable and sustainable superhydrophobic surface with intertwined cellulose/SiO_2 blends for anti-icing and self-cleaning applications [J]. Materials & Design, 2022, 217: 110628.

[23] CHEN Xiao-tong, WANG Peng, ZHANG Dun, WU Jia-jia, OU Jun-fei. How surface orientation affects coalescence-induced droplet jumping behavior and subsequent atmospheric corrosion resistance of a superhydrophobic surface? [J]. Corrosion Science, 2022, 197: 110082.

[24] MENG Xue, WANG Jin-lei, ZHANG Jie, NIU Bao-long, GAO Xiang-hua, YAN Hong. Electroplated super-hydrophobic Zn−Fe coating for corrosion protection on magnesium alloy [J]. Transactions of Nonferrous Metals Society of China, 2022, 32(10): 3250−3258.

[25] LI Xue-wu, YAN Jia-yang, YU Teng, ZHANG Bin-bin. Versatile nonfluorinated superhydrophobic coating with self-cleaning, anti-fouling, anti-corrosion and mechanical stability [J]. Colloids and Surfaces A: Physicochemical and Engineering Aspects, 2022, 642: 128701.

[26] DENG Wen, AN Yu-long, ZHAO Xiao-qin, ZHANG Chang-fu, TANG Lin, LIU Jun-qiang. Cavitation erosion behavior of ceramic/organic coatings exposed to artificial seawater [J]. Surface and Coatings Technology, 2020, 399: 126133.

[27] LI Guo, YUE Jiang, GUO Chen-hao, JI Yong-sheng. Influences of modified nanoparticles on hydrophobicity of concrete with organic film coating [J]. Construction and Building Materials, 2018, 169: 1−7.

[28] NAMBAFU G S, KIM N, KIM J Y. Hydrophobic coatings prepared using various dipodal silane-functionalized polymer precursors [J]. Applied Surface Science Advances, 2022, 7: 100207.

[29] PAL S, MONDAL S, PAL P, DAS A, MAITY J. Fabrication of AgNPs/silane coated mechanical and washing durable hydrophobic cotton textile for self-cleaning and oil−water separation application [J]. Journal of the Indian Chemical Society, 2022, 99(1): 100283.

[30] HU Hui-li, LI Ning, ZHU Yong-ming. Effect of chromate on the electrochemical behavior of sintered Zn−Al coating in seawater [J]. Surface and Coatings Technology, 2008, 202(24): 5847−5852.

[31] LIU Jian-guo, GONG Gao-ping, YAN Chuan-wei. EIS study of corrosion behaviour of organic coating/dacromet composite systems [J]. Electrochimica Acta, 2005, 50(16/17): 3320−3332.

[32] ZHANG Ke-bing, ZHANG Ming-ming, QIAO Jing-fei, ZHANG Sheng-lin. Enhancement of the corrosion resistance of zinc−aluminum−chromium coating with cerium nitrate [J]. Journal of Alloys and Compounds, 2017, 692: 460−464.

[33] SANTIAGO A A G, GONDIM J G S, TRANQUILIN R L, SILVA F S, FERNANDEZ F F, COSTA M C B, MOTTA F V, BOMIO M R D. Development of ZnO/PDMS nano-composite with photocatalytic/hydrophobic multifunction [J]. Chemical Physics Letters, 2020, 740: 137051.

[34] NING Wei-jie, YANG Ya-wen, ZHANG Ding, PAN Ren-ming. Surface modification of sodium bicarbonate ultrafine power extinguishing agent by environmental friendly fluorinated acrylate copolymers [J]. Polymer Degradation and Stability, 2021, 187: 109558.

[35] SONG Qing, ZHAO Rui-xiang, LIU Tong, GAO Ling-ling, SU Cui-cui, YE Yu-min, CHAN Siew-Yin, LIU Xin-yue, WANG Ke, LI Peng, HUANG Wei. One-step vapor deposition of fluorinated polycationic coating to fabricate antifouling and anti-infective textile against drug-resistant bacteria and viruses [J]. Chemical Engineering Journal, 2021, 418: 129368.

[36] JIANG J Y, XU J L, LIU Z H, DENG L, SUN B, LIU S D, WANG L, LIU H Y. Preparation, corrosion resistance and hemocompatibility of the superhydrophobic TiO_2 coatings on biomedical Ti−6Al−4V alloys [J]. Applied Surface Science. 2015, 347: 591−595.

[37] ZHANG L W, XU J L, CHEN J, HUANG J, LUO J M. Microstructure and corrosion resistance of AlCoCrFeNi high-entropy alloy coating on sintered NdFeB magnets prepared by HVOF spraying [J]. Journal of Magnetism and Magnetic Materials, 2022, 551: 169136.

[38] TAO Lei, LI He-qin, SHEN Jiong, QIAO Kai, WANG Wei, ZHOU Chu, ZHANG Jing, TANG Qiong. Corrosion resistance of the NdFeB coated with AlN/SiC bilayer thin films by magnetron sputtering under different environments [J]. Journal of Magnetism and Magnetic Materials, 2015, 375: 124−128.

[39] HU Cheng-lu, LE Qi-chi, ZHOU Xiong, CHENG Chun-long, GUO Rui-zhen, LI Xiao-qiang, LI Dan-dan, ZHANG

Xin-yue. The growth and corrosion mechanism of Zn-based coating on AZ31 magnesium alloys by novel hot-dip process [J]. Materials Characterization, 2022, 189: 111988.

[40] HOANG N, KHOA T A, NHUNG L T, PHUONG P M, HANG T T X, van CHI N, NGUYEN T D. Corrosion protection of carbon steel using a combination of Zr conversion coating and subsequent zinc-rich silicate coating with a flake ZnAl alloy [J]. Arabian Journal of Chemistry, 2022, 15(6): 103815.

[41] LIU Xiao-xiao, KONG De-jun. Salt spray corrosion and electrochemical corrosion performances of Dacromet fabricated Zn−Al coating [J]. Anti-Corrosion Methods and Materials, 2019, 66(5): 565−572.

[42] RAJKUMAR R, VEDHI C. A study of corrosion protection efficiency of silica nanoparticles acrylic coated on mild steel electrode [J]. Vacuum, 2019, 161: 1−4.

[43] SHI Xiao-ting, WANG Yu, LI Hong-yu, ZHANG Shu-fang, ZHAO Rong-fang, LI Guo-qiang, ZHANG Rong-fa, SHENG Yang, CAO Si-yue, ZHAO You-jun, XU Lin-na, ZHAO Ying. Corrosion resistance and biocompatibility of calcium-containing coatings developed in near-neutral solutions containing phytic acid and phosphoric acid on AZ31B alloy [J]. Journal of Alloys and Compounds, 2020, 823: 153721.

[44] QIN Jin, SHI Xiao-ting, LI Hong-yu, ZHAO Rong-fang, LI Guo-qiang, ZHANG Shu-fang, DING Li-yun, CUI Xue-jun, ZHAO Ying, ZHANG Rong-fa. Performance and failure process of green recycling solutions for preparing high degradation resistance coating on biomedical magnesium alloys [J]. Green Chemistry, 2022, 24: 8113−8130.

烧结 NdFeB 磁体表面 Zn−Al/T8 超疏水复合涂层的显微组织及耐蚀性

张晓虎，罗军明，徐吉林，陈 金，黄 俊，马永存，薛名山

南昌航空大学 材料科学与工程学院，南昌 330063

摘 要：为提升烧结 NdFeB 磁体的耐蚀性，采用旋涂法和等离子体增强化学气相沉积技术在其表面制备 Zn−Al/T8 (2-全氟辛基乙基丙烯酸酯)超疏水复合涂层。结果表明，Zn−Al 涂层主要由片层状的 Zn 和 Al 相组成，厚度大约为 28 μm。Zn−Al/T8 复合涂层的接触角达到 151.78°，而滚动角仅为 5.13°，说明 Zn−Al/T8 复合涂层可提供一个超疏水表面。Zn−Al 涂层和 Zn−Al/T8 复合涂层对烧结 NdFeB 的磁性能均无显著影响。Zn−Al 涂层通过牺牲阳极来提高 NdFeB 磁体的耐蚀性，而 Zn−Al/T8 复合涂层通过超疏水表面进一步提升耐蚀性。Zn−Al/T8 复合涂层较 Zn−Al 涂层具有更好的耐盐雾性能。Zn−Al/T8 超疏水复合涂层是一种非常有前途的烧结 NdFeB 磁体保护涂层。

关键词：显微组织；耐蚀性；烧结 NdFeB 磁体；Zn−Al 涂层；超疏水表面；旋涂法；等离子体增强化学气相沉积

(Edited by Xiang-qun LI)